

Long-Lived Sleptons at the LHC and a 100 TeV Proton Collider

Jonathan L. Feng,¹ Sho Iwamoto,² Yael Shadmi,² and Shlomit Tarem²

¹*Department of Physics and Astronomy,
University of California, Irvine, CA 92697, USA*

²*Physics Department, Technion—Israel Institute of Technology, Haifa 32000, Israel*

Abstract

We study the prospects for long-lived charged particle (LLCP) searches at current and future LHC runs and at a 100 TeV pp collider, using Drell–Yan slepton pair production as an example. Because momentum measurements become more challenging for very energetic particles, we carefully treat the expected momentum resolution. At the same time, a novel feature of 100 TeV collisions is the significant energy loss of energetic muons in the calorimeter. We use this to help discriminate between muons and LLCs. We find that the 14 TeV LHC with an integrated luminosity of 3 ab^{-1} can probe LLCP slepton masses up to 1.2 TeV, and a 100 TeV pp collider with 3 ab^{-1} can probe LLCP slepton masses up to 4 TeV, using time-of-flight measurements. These searches will have striking implications for dark matter, with the LHC definitively testing the possibility of slepton–neutralino co-annihilating WIMP dark matter, and with the LHC and future hadron colliders having a strong potential for discovering LLCs in models with superWIMP dark matter.

PACS numbers: 12.60.Jv, 95.35.+d, 13.85.-t

I. INTRODUCTION

Many extensions of the standard model (SM) predict long-lived charged particles (LLCPs) that are stable on collider-detector timescales. Such particles present new challenges for collider experiments, requiring novel methods for triggering, reconstruction, and detection. At the same time, their discovery would be extremely exciting, with profound implications for both particle physics and cosmology. In addition, LLCPs would provide nearly background-free handles to discover heavier new particles, if these exist. For these reasons, LLCP searches have attracted great interest in recent years, culminating in new limits on LLCP masses from experiments at the 7 and 8 TeV LHC [1–3].

In this paper, we investigate the capabilities of current and future high luminosity runs of the LHC for discovering LLCPs, as well as the potential of a future 100 TeV hadron collider for LLCP searches. Because of the unique methods required for their detection, LLCP searches provide an interesting testing ground for future colliders and detectors. In addition, LLCP cosmology and its implications for future colliders are worth considering. Cosmology is well-known to provide constraints that are complementary to conventional particle physics bounds. For example, requiring that thermal relic neutralinos not overclose the Universe implies an *upper* bound on neutralino masses. The possibility of completely probing the viable thermal relic neutralino dark matter (DM) parameter space is therefore useful input to setting a target center-of-mass energy for future pp colliders [4–7]. LLCPs may also play key roles in cosmology; for example, they may decay to DM particles and thereby affect the DM relic abundance. Here we determine the implications of cosmological scenarios with LLCPs for future collider energies and detector design.

We will concentrate on a worst-case scenario, in which the only new particle within reach is a non-colored LLCP, which we will take to be a slepton. Our results are thus based on Drell–Yan slepton pair production and can be trivially generalized to pair production of LLCPs with different quantum numbers. Furthermore, these results are very robust and do not depend on the assumption of supersymmetry.

At the same time, supersymmetry provides at least two well-motivated frameworks for LLCPs. One is gauge-mediated supersymmetry breaking, in which the lightest supersymmetric particle (LSP) is the gravitino, and the next-to-lightest supersymmetric particle (NLSP) is a charged slepton [8–10]. The reach of the 100 TeV collider for first generation squarks and gluinos has been estimated to be 10–15 TeV [11]. As we discuss below, if these particles are beyond reach, the supersymmetry scale must be high, with the gravitino mass \gtrsim MeV and quite possibly much higher than that and in the GeV to TeV range. This entire range of gravitino masses generically results in a long-lived slepton NLSP. From the point of view of cosmology, this scenario provides a realization of superweakly-interacting massive particle (superWIMP) DM, with metastable sleptons decaying to gravitinos, which form superWIMP DM [12, 13].

A second framework of interest is the slepton–neutralino co-annihilation scenario, in which a small slepton–neutralino mass difference is motivated by DM [14, 15]. Here DM is the neutralino LSP, and its relic abundance is diluted through co-annihilations with a quasi-degenerate slepton. Slepton decay to the LSP is thus phase-space suppressed. The correct relic abundance is obtained for slepton masses \lesssim 600 GeV. We will find that, in agreement with Refs. [16, 17], the entire cosmologically-motivated mass range can be probed by the 14 TeV LHC.

Non-colored LLCPs interact in the detector much like muons. Thus, the main challenge in

their discovery is distinguishing them from muons. ATLAS and CMS rely both on differences in the energy loss (dE/dx) of LLCs and muons in the inner detectors, and on time-of-flight (ToF) measurements in the muon detectors. In this study, we will only consider the latter, essentially extrapolating from what has been done at the LHC¹. At a 100 TeV collider, however, we have a qualitatively new handle at our disposal, since energetic muons lose energy through radiative processes, i.e., bremsstrahlung, electron pair-production, and photo-nuclear interactions [20], in addition to ionization. In contrast, the radiative energy loss would be negligible for a heavy LLC. We therefore cut on the energy measured in the calorimeter along the track of the candidate, to reduce the number of background muons.

As noted above, a 100 TeV collider may provide a definitive test of (stable) supersymmetric WIMP DM [4–7]. We will find that the superWIMP DM scenario is harder to probe exhaustively, since the DM relic abundance does not provide a strict upper bound on the slepton mass—increasing the slepton mass can in principle be compensated by decreasing the gravitino mass. In the framework we consider here, the lower bound on the slepton lifetime \gtrsim nsec, implies a *model-independent* upper bound on the slepton mass around 40 TeV, which is, of course, beyond the reach of any foreseeable collider. Still, as we will see, the 100 TeV collider with 3 ab^{-1} could probe sleptons with masses up to 3.2 to 4.0 TeV, depending on the left–right composition of the sleptons. The testable mass range therefore includes a wide range of cosmologically-allowed models, including the interesting region of superWIMP models in which late slepton decays may have measurable effects on big bang nucleosynthesis (BBN) or the cosmic microwave background (CMB). As noted above, the worst-case scenario we consider, with colored superpartners beyond reach, implies a high supersymmetry-breaking scale, which is precisely the relevant region for the 100 TeV collider LLC searches.

This paper is organized as follows. In Sec. II we review the two long-lived slepton scenarios discussed above and summarize the relevant mass ranges. In Sec. III, we discuss LLC collider searches, starting with a detailed description of our analysis of the 14 TeV LHC in Sec. III A, and providing an overview of our Monte Carlo simulation. We then go on to discuss the 100 TeV collider in Sec. III B, where we review the proposed detector, discuss novel features at these extreme energy scales, and study the prospects for LLC searches at 100 TeV. The results are discussed in Sec. IV. We conclude with a collection of the results and some remarks in Sec. V. Details of the Monte Carlo simulations are collected in the Appendix.

II. TARGET MASS RANGES FROM COSMOLOGY

The search for LLCs is important independent of any theoretical framework, and the searches described in the following sections are in fact model-independent. At the same time, it is useful to have some scenarios with target mass ranges in mind to motivate the searches. In this section, we highlight two cosmological scenarios that point to particularly interesting mass ranges for long-lived sleptons.

¹ The LHC reach for long-lived slepton was also studied in [18, 19], selecting sleptons with speeds $0.6 < \beta < 0.8$ to discriminate them from muons. Here we select a wider range of slepton β , based on current ATLAS searches.

A. Slepton SuperWIMP Scenarios

Sleptons may be long-lived, because their decays are mediated by very weak interactions. Perhaps the most generic possibility is the superWIMP scenario [12, 13] with slepton NLSPs that decay to gravitino LSPs, in which the decays are suppressed by the weakness of gravity. The gravitinos then comprise part, or all, of DM.

The width for the decay of a slepton to a gravitino is [21]

$$\Gamma(\tilde{l} \rightarrow l\tilde{G}) = \frac{1}{48\pi M_*^2} \frac{m_{\tilde{l}}^5}{m_{\tilde{G}}^2} \left[1 - \frac{m_{\tilde{G}}^2}{m_{\tilde{l}}^2} \right]^4, \quad (1)$$

where $M_* \simeq 2.4 \times 10^{18}$ GeV is the reduced Planck mass, assuming the lepton mass is negligible. When the gravitino is much lighter than the slepton, the slepton lifetime is

$$\tau(\tilde{l} \rightarrow l\tilde{G}) \simeq 5.7 \times 10^{-7} \text{ sec} \left(\frac{\text{TeV}}{m_{\tilde{l}}} \right)^5 \left(\frac{m_{\tilde{G}}}{\text{MeV}} \right)^2, \quad (2)$$

and for $m_{\tilde{l}} \sim \text{TeV}$ and $m_{\tilde{G}} \gtrsim \text{MeV}$, the slepton is effectively stable in collider experiments.

In superWIMP scenarios, the NLSP first freezes out with relic density given approximately by [22, 23]

$$\Omega_{\text{NLSP}}^{\text{th}} h^2 \approx \frac{1.1 \times 10^9 x_F \text{ GeV}^{-1}}{\sqrt{g_*} M_{\text{Pl}} \langle \sigma v \rangle} \approx 0.2 \left[\frac{15}{\sqrt{g_*}} \right] \left[\frac{x_f}{30} \right] \left[\frac{10^{19} \text{ GeV}}{M_{\text{Pl}}} \right] \left[\frac{10^{-9} \text{ GeV}^{-2}}{\langle \sigma v \rangle} \right], \quad (3)$$

where g_* is the effective number of massless degrees of freedom at freeze out, $x_f \equiv m_{\text{NLSP}}/T_f \approx 25$ is the NLSP mass divided by the freeze out temperature T_f , $M_{\text{Pl}} \simeq 1.2 \times 10^{19}$ GeV is the (unreduced) Planck mass, and $\langle \sigma v \rangle$ is the thermally-averaged NLSP annihilation cross section. Let us assume that the NLSPs are right-handed sleptons \tilde{l}_R , and the number of slepton generations among $\tilde{e}_R, \tilde{\mu}_R$ and $\tilde{\tau}_R$ that are degenerate and long-lived is $N_{\text{gen;LL}}$, where $1 \leq N_{\text{gen;LL}} \leq 3$. (It is not difficult to generalize this to scenarios with left-handed slepton NLSPs.) The dominant annihilation channels are typically $\tilde{l}\tilde{l}^* \rightarrow \gamma\gamma, \gamma Z, ZZ$ through slepton exchange and $\tilde{l}\tilde{l} \rightarrow ll$ through Bino exchange. For right-handed sleptons, the thermally-averaged cross section near threshold is approximately [24]

$$\langle \sigma v \rangle \approx \frac{4\pi\alpha^2}{m_{\tilde{l}_R}^2} + \frac{16\pi\alpha^2 m_{\tilde{B}}^2}{\cos^4 \theta_W (m_{\tilde{l}_R}^2 + m_{\tilde{B}}^2)^2} \equiv C_{\tilde{B}} \frac{4\pi\alpha^2}{m_{\tilde{l}_R}^2}, \quad (4)$$

where $m_{\tilde{B}}$ and $m_{\tilde{l}_R}$ are the Bino and slepton masses, respectively, and $C_{\tilde{B}}$ is 1 for infinitely heavy Bininos and increases monotonically to $C_{\tilde{B}} \simeq 2.7$ as the Bino mass decreases from infinity to near the slepton mass.

When the slepton decays to the gravitino $\tilde{l}_R \rightarrow l\tilde{G}$, the gravitino inherits the relic density

$$\Omega_{\tilde{G}} h^2 = \frac{m_{\tilde{G}}}{m_{\tilde{l}_R}} \Omega_{\text{NLSP}}^{\text{th}} h^2 \quad (5)$$

from each slepton. Combining Eqs. (3), (4), and (5), we find that, numerically, the gravitino relic density is

$$\Omega_{\tilde{G}} h^2 = N_{\text{gen;LL}} \cdot 0.12 \frac{m_{\tilde{l}_R} m_{\tilde{G}}}{M^2}, \quad (6)$$

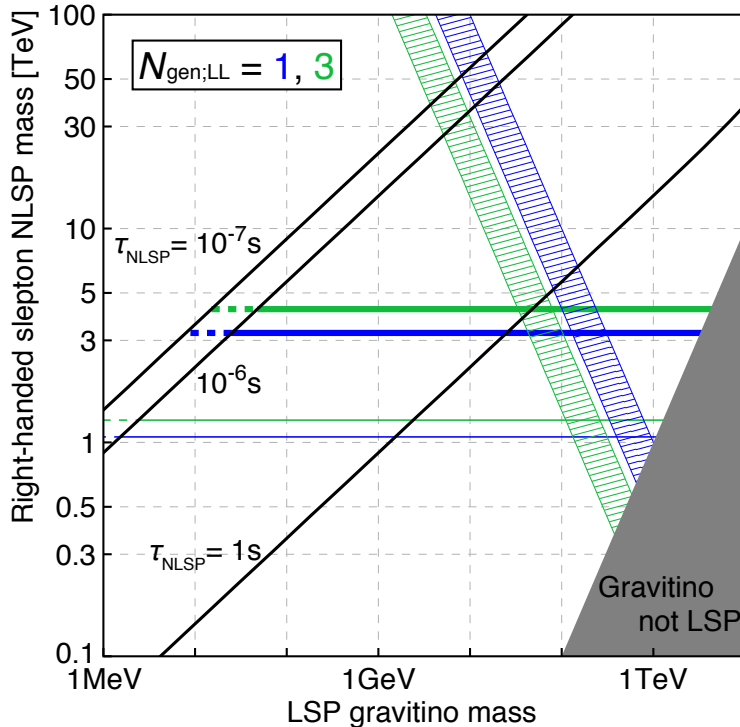


FIG. 1: An overview of the parameter space in superWIMP scenarios. The black lines illustrate the lifetime of the NLSP slepton $\tau_{\text{NLSP}} = 10^{-7}$, 10^{-6} and 1 sec. In the blue (green) hatched region, gravitinos saturate the DM relic density if $N_{\text{gen;LL}} = 1$ (3), i.e., one (three) right-handed slepton is long-lived. The upper and lower edges of the regions correspond to $m_{\tilde{B}} \sim m_{\tilde{l}_R}$ and $m_{\tilde{B}} \gg m_{\tilde{l}_R}$, respectively. The horizontal lines are the expected reach of right-handed long-lived slepton searches: the thinner lines are the expected exclusion limits at the 14 TeV LHC, and the thicker lines are the expected exclusion limits at a 100 TeV collider, both with an integrated luminosity of 3 ab^{-1} .

where M varies from 650 GeV to 1.0 TeV for Bino masses varying from $m_{\tilde{B}} = \infty$ to $m_{\tilde{l}_R}$. For $m_{\tilde{l}_R} \sim m_{\tilde{G}}$, the relic abundance is saturated when both masses are around 600 GeV. If, on the other hand, the gravitino is much lighter than the slepton, the constraint that the slepton be long-lived, with, say, $\tau_{\text{NLSP}} \geq 10^{-6} \text{ sec}$ ², implies

$$\frac{m_{\tilde{l}_R}}{\text{TeV}} \lesssim \left(\frac{m_{\tilde{G}}}{\text{MeV}} \right)^{2/5}. \quad (7)$$

The DM abundance then provides a *model-independent* upper limit on the slepton mass in this scenario,

$$m_{\tilde{l}_R} \lesssim 40 \text{ TeV}, \quad (8)$$

which is beyond the reach of any foreseeable experiment.

We display the results above in Fig. 1, in the slepton–gravitino mass plane. In the blue (green) hatched regions, gravitinos from late slepton decays saturate the DM abundance for one (three degenerate) long-lived sleptons, depending on the Bino mass. The upper

² A somewhat smaller value, say, $5 \times 10^{-7} \text{ sec}$ is probably safe, too, but shorter lifetimes will lead to smaller efficiencies, as some of the sleptons may decay in the detectors.

(lower) edges correspond to $m_{\tilde{B}} \sim m_{\tilde{t}_R}$ ($m_{\tilde{B}} \gg m_{\tilde{t}_R}$), i.e., $C_{\tilde{B}} = 2.7$ (1.0) in Eq. (4), and $M/\sqrt{N_{\text{gen;LL}}} = 1$ TeV (650 GeV) in Eq. (6). The region of the plane above the upper edge is excluded by DM overabundance.

The black lines correspond to different slepton lifetimes. Above the 10^{-7} – 10^{-6} sec lines, some sleptons decay inside the detector, and the efficiency of the searches described here deteriorates. (Of course, this may lead to spectacular signals in other channels.) Also shown is the $\tau_{\text{NLSP}} \sim \text{sec}$ line, below which BBN and CMB constraints become relevant. For such long decay times, the SM particles produced in slepton decays are not quickly thermalized, and they may destroy light elements or modify the black body spectrum of the CMB [12, 13, 21, 25–27]. These effects may be in conflict with the successes of standard BBN or observations of the CMB, excluding some late decay scenarios. On the other hand, in some cases, the late decays may alleviate discrepancies between the predictions of standard BBN and the observed abundances, particularly of ${}^7\text{Li}$ and ${}^6\text{Li}$. In any case, it is clear that LLCPP collider probes of the region of parameter space with slepton lifetimes longer than 1 second may have particularly interesting implications for the early Universe.

Finally, we also show in this figure the main results of the analysis of Secs. III A and III B, namely, the projected reach of the 14 TeV LHC and 100 TeV pp collider. These are given by the horizontal lines, the thinner for the 14 TeV LHC and the thicker for the 100 TeV collider, where again, the blue (green) line corresponds to one (three degenerate) right-handed sleptons. We see that collider searches can probe a significant portion of the allowed parameter space, including most of the superWIMP parameter space with lifetimes longer than a second, which, as explained above, is especially interesting.

In fact, the region which could be probed by a 100 TeV collider is also well-motivated by more theoretical considerations. Recall that we assume here that squark and gluino masses are above 10 TeV and beyond the reach of a 100 TeV collider. In gauge-mediation, these masses are roughly given by

$$10^{-2} \frac{F_{\text{GMSB}}}{M_{\text{mess}}}, \quad (9)$$

with $M_{\text{mess}}^2 > F_{\text{GMSB}}$. Thus, both the messenger scale M_{mess} and the supersymmetry breaking F_{GMSB} are pushed to high values. The gravitino mass is given by

$$m_{\tilde{G}} \sim \frac{F_0}{M_{\text{Pl}}} \equiv c_{\text{grav}} \frac{F_{\text{GMSB}}}{M_{\text{Pl}}}, \quad (10)$$

where F_0 is the dominant supersymmetry-breaking F -term. The number c_{grav} depends on the details of the supersymmetry breaking sector; the most concrete, calculable models predict $c_{\text{grav}} \gg 1$. Combining these, we see that $m_{\tilde{G}} \gtrsim 1$ MeV, with values of 1–100 GeV perhaps even more plausible, and so TeV-mass sleptons are necessarily long-lived on collider-detector timescales.

Let us briefly discuss the limit obtained at the 8 TeV LHC, which is not shown in the figure. Assuming only Drell–Yan direct pair production of a single generation slepton ($N_{\text{gen;LL}} = 1$), the CMS (ATLAS) Collaboration excludes long-lived sleptons with masses $m < 346$ (286) GeV [1, 2], which does not exclude any of the region suggested in the SuperWIMP scenario (the hatched region). For $N_{\text{gen;LL}} = 3$, the ATLAS Collaboration excludes $m < 337$ GeV, and the CMS analysis excludes $m \lesssim 440$ GeV, which slightly overlaps the cosmologically-favored region.

B. Slepton–Neutralino Co-Annihilation

Sleptons may be long-lived because their decay rate is phase-space suppressed. Perhaps the best motivation for such phase-space suppression is the slepton–neutralino co-annihilation scenario, in which neutralinos freeze out and are DM, and their thermal relic density is reduced to viable levels through co-annihilation with highly degenerate sleptons.

This has recently been explored in detail in Refs. [16, 17] in the CMSSM framework, where there is a cosmologically-preferred stau–neutralino co-annihilation region of parameter space, but the resulting ranges of neutralino and stau masses hold more generally, since they are driven by the DM relic abundance. For stau–neutralino splittings less than about 1 GeV, the staus are long-lived at colliders, and the correct relic density can be obtained for gaugino masses $M_{1/2} \sim 800\text{--}1400$ GeV, where the exact value depends on $\tan\beta$ and the A -parameter that determines the left–right stau mixing. This scenario therefore motivates stau masses

$$m_{\tilde{\tau}} \simeq m_{\chi} \simeq 0.42M_{1/2} \approx 350\text{--}600 \text{ GeV} . \quad (11)$$

This range is just being probed by current bounds. The upper bound is achieved for exactly degenerate staus and neutralinos, where the co-annihilation effect is maximized, and so this is a hard upper bound in this scenario: heavier staus will necessarily overclose the Universe.

III. LLCP COLLIDER SEARCHES

In collider experiments, metastable sleptons, or more generally non-colored LLCs, interact with the detectors much like muons. An LLC passes through the detector, leaving a charged track from ionization energy loss, with small energy deposits in the calorimeters. Therefore, the main background is muons, and the only difference between a hypothetical LLC and a muon is the (assumed) large mass of the former. Because of this large mass, LLCs would typically be produced with a smaller speed β . This speed can be measured using the ToF to the outer detectors, or the ionization energy loss, dE/dx , which depends on $\beta\gamma$, with $\gamma = (1 - \beta^2)^{-1/2}$. The ATLAS and CMS collaborations have used both of these methods at the LHC with $\sqrt{s} = 7\text{--}8$ TeV, but here we will only consider ToF measurements, for which the specifics of the detector are less relevant.

At very high energies, the LLC mass leads to an additional qualitative difference between LLCs and muons: while TeV-energy muons lose significant energy through radiative processes, LLCs do not. This can provide a useful handle for discriminating LLCs from muons at future high energy colliders.

As noted above, we consider a worst-case scenario in which the only new particles produced are slepton LLCs. The signal is, then, Drell–Yan slepton pair production, and we will consider three different slepton types: purely left-handed sleptons, which we denote \tilde{e}_L , purely right-handed sleptons \tilde{e}_R , and left–right mixed sleptons, which we denote $\tilde{\tau}_1$. Note that slepton flavor does not matter here, since the slepton does not decay in the detector³.

In the following we will study the prospects for slepton detection at a 100 TeV collider, as compared to the 14 TeV LHC. There is no concrete design, at this point, of the detectors

³ If other superpartners are also within reach, production of these particles would lead to much higher reach in the LLC mass because such events typically include at least two LLCs with accompanying visible particles. Note that the β distributions of such LLCs tend to be stiffer.

that will be deployed at a 100 TeV collider. Furthermore, detector techniques are expected to improve before such a design is made. We therefore make several simplifying assumptions. The main one is that the detector will measure the momenta of high-momentum particles produced at $\sqrt{s} = 100$ TeV as well as the LHC detectors perform for particles with momenta up to 1 TeV. A second assumption is that new advances will allow good resolution at high pile-up, or that the collider will not run at luminosities so high that the pile-up will prevent good reconstruction.

The uncertainty regarding the detector performance far outweighs the effects of systematic uncertainties, on the order of 10–20%, that were assigned in the LHC Run 1 searches [1, 2]. Thus, for meaningful comparison of the 14 TeV and 100 TeV searches, we do not consider systematic uncertainties in this work.

A. LLCP Searches at the 14 TeV LHC

1. Monte Carlo Simulation

We use the Snowmass background set for 14 TeV pp colliders [28–30], which is briefly described in the Appendix, to estimate SM background. We generate our signal events, slepton Drell–Yan pair production, with the same tools used to generate the background set. The pair production is calculated at tree-level using `MadGraph5_aMC@NLO` [31], with showering and hadronization performed by `Pythia6` [32] with the `Pythia-PGS` interface. For the detector simulation we use `Delphes` tuned by the Snowmass Collaboration based on `Delphes 3.0.9` [33–35]. The momentum resolution of muons is assumed to be $\Delta P_T = 0.05 P_T$ for $P_T > 200$ GeV. Pileup is not considered.

Because the ToF measurement is used to distinguish sleptons from muons, its resolution is carefully treated. At the ATLAS detector, the resolution of ToF is reported as 2.5% [2]. This is the value we use for the slepton speed measurement. Thus, the slepton speed is smeared according to

$$\text{PDF}(\hat{\beta}^{-1})_{\tilde{l}} = \text{N}(\beta^{-1}, 0.025), \quad (12)$$

where $\hat{\beta}$ is the smeared slepton speed, and $\text{N}(\mu, \sigma)$ is the Normal distribution with mean μ and dispersion σ . For muons, however, this distribution is inaccurate, because the dominant background comes from the tail of the distribution. We therefore use a more detailed distribution for the muons' $\hat{\beta}$,

$$\text{PDF}(\hat{\beta})_{\mu} = 0.832 \cdot \text{N}(1, 0.022) + 0.162 \cdot \text{N}(1, 0.050) + 0.00534 \cdot \text{N}(1, 0.116), \quad (13)$$

which is obtained by fitting the measured β distribution at the ATLAS experiment (Fig. 1 of Ref. [2]).

After object identification performed by `Delphes`, all objects with $P_T < 30$ GeV are dropped, and muon pairs are removed if their invariant masses satisfy $|m_{\mu\mu} - m_Z| < 5$ GeV. The remaining muons are tagged as LLCPs if they satisfy the following conditions:

- $P_T > 100$ GeV and $|\eta| < 2.4$,
- $\Delta R > 0.5$ from the nearest reconstructed object (with $P_T > 30$ GeV),
- $0.3 < \hat{\beta} < 0.95$,

where $\hat{\beta}$ is the smeared speed as defined above.

The accurate measurement of the speed β is a result of quality requirements made on the reconstructed tracks and timing measurements. Following the results of the ATLAS selection, we assign quality selection efficiencies of $\epsilon_\mu = 0.5$ for identifying a fake LLCP (muon), and $\epsilon_{\tilde{l}} = 0.6$ for a true LLCP (slepton)⁴.

We select events with two LLCP candidates. If the event has more than two LLCP candidates, the two with the highest P_T 's are used. For each LLCP, we calculate the reconstructed mass

$$\hat{m} = \frac{P_T \cosh \eta}{\hat{\beta} \hat{\gamma}}, \quad (14)$$

where $\hat{\gamma} = (1 - \hat{\beta}^2)^{-1/2}$.

We define eight signal regions (SRs): SR300, SR400, \dots , SR1000, where SR x requires both of the LLCPs to have $\hat{m} > x$ GeV. For each signal region, the expected 95% confidence level (CL) upper limit on the number of events, N_{UL} , is calculated with the CL_s method [36]. Based on N_{UL} , the corresponding upper limit on the signal cross section, σ_{UL} , is calculated for different LLCP scenarios. Because of the inclusive SR definition, the lowest σ_{UL} gives the limit on the scenario. Statistical uncertainties are considered, but systematic uncertainties are not included in this analysis.

2. Results

The LLCP selection flow is shown in Table I for several LLCP masses, together with the total cross sections and the cross sections for events with one and two tagged LLCPs. Note that the signal is calculated at LO, while the background is calculated at NLO. The efficiency factors ϵ_μ and $\epsilon_{\tilde{l}}$ are not imposed in this table for simplicity.

In Table II, we show the separate contributions in each of the signal regions, with the different efficiencies for sleptons and fake LLCPs included. We also display N_{UL} for integrated luminosities of $\int \mathcal{L} = 0.1, 0.3, \text{ and } 3 \text{ ab}^{-1}$. Tighter SRs are mostly background free, and result in $N_{\text{UL}} \simeq 3.0$ because of the statistical uncertainty due to the Poisson distribution.

The results of this analysis are shown in Fig. 2. The upper bound σ_{UL} (black solid lines) on the signal cross section is computed for integrated luminosities $\int \mathcal{L} = 0.1, 0.3, \text{ and } 3 \text{ ab}^{-1}$. The statistical uncertainty is indicated by the green and yellow bands; the observed limits would fall in the green (yellow) band with a probability of 68% (95%). To quantify the effect of systematic uncertainties on the background, we calculated σ_{UL} with the background contribution multiplied by five (black dashed lines).

The signal cross sections are also given by the solid contours. That for left- (right-) handed sleptons is drawn by the red (blue) contour. For the left–right mixed slepton $\tilde{\tau}_1$, the Drell–Yan production cross section is maximized in the case where $\tilde{\tau}_1$ coincides with $\tilde{\tau}_L$, and minimized for $\theta \simeq 1.1$, where we define $\tilde{\tau}_1 = \tilde{\tau}_L \cos \theta + \tilde{\tau}_R \sin \theta$. Thus the cross section at $\theta = 1.1$ is given by the solid magenta line, so that the expected reach of mixed slepton LLCP search lies between the magenta and red lines for any value of θ .

We see that, for $N_{\text{gen;LL}} = 1$, long-lived left-handed (right-handed) sleptons below ~ 800 (700) GeV can be excluded by Run 2 of the LHC with $\int \mathcal{L} = 0.3 \text{ ab}^{-1}$, and below

⁴ The efficiency for fake LLCP identification is worse than for true LLCP identification, because a poorly measured β is uncorrelated between sub-detectors, and may be correlated with a poor-quality track.

TABLE I: LLCP selection flow and cross section of events in the 14 TeV LHC analysis, for \tilde{e}_L pair-production ($N_{\text{gen;LL}} = 1$). The efficiency factors ϵ_μ and ϵ_τ are not included. SM background (BKG) is calculated with NLO cross sections, while signal cross sections are based on Drell–Yan production at tree-level. We show the number of LLCP candidates for LLCP selection flow, and the number of events for event cross section.

	signal ($pp \rightarrow \tilde{e}_L \tilde{e}_L^*$) with $m_{\tilde{e}_L} =$				SM BKG
	400 GeV	600 GeV	800 GeV	1 TeV	—
LLCP selection flow [ab]					
candidates	2.31×10^3	359	80.5	21.9	—
+ $P_T > 100$ GeV, isolated	2.08×10^3	337	76.4	20.9	1.06×10^8
+ $0.3 < \hat{\beta} < 0.95$	1.77×10^3	312	73.9	20.6	3.92×10^6
Event cross section [ab]					
total cross section	1.15×10^3	180	40.2	10.9	—
$N_{\text{LLCP}} = 1$	320	35.8	5.55	1.10	3.92×10^6
$N_{\text{LLCP}} = 2$	727	138	34.2	9.74	1.29×10^3

~ 1.2 (1.1) TeV at the high-luminosity LHC (HL-LHC) with $\int \mathcal{L} = 3 \text{ ab}^{-1}$. These numbers assume single slepton production. Left–right mixed sleptons can be excluded for $m_{\text{UL}} \simeq 700\text{--}800$ GeV, depending on the mixing angle, in Run 2, and for 1.1–1.2 TeV at the HL-LHC.

It is also interesting to consider scenarios with two or more (nearly-) degenerate sleptons. For example, if the right-handed selectron and smuon are degenerate and long-lived, the limits on their mass would increase to 0.8 (1.2) TeV with $\int \mathcal{L} = 0.3$ (3) ab^{-1} .

B. LLCP Searches at a 100 TeV pp Collider

1. Detector Assumptions and General Considerations

We now proceed to analyze slepton pair production in a 100 TeV collider. We assume a detector that is roughly like ATLAS or CMS, with the collision point and the beam pipe surrounded by an inner detector (ID) for tracking, followed by calorimeters, and with the muon spectrometer (MS) as the outermost layer. We utilize only the region $|\eta| \lesssim 2.5$ ⁵.

The detectors should meet the following two conditions to achieve good object reconstruction and particle identification. First, the calorimeters should be thick and dense enough to stop electrons, photons, and hadrons, which guarantees good muon observation at the MS. Second, the magnetic fields inside the trackers should be large enough to bend energetic charged particles. As we see below, the momentum resolution is determined by the field strength. LLCPs are observed as slow muons, and searched for using ToF techniques employed at Run 1 of the LHC, which we reviewed at the beginning of Sec. III.

In 100 TeV collisions, however, two new features are expected. First, muons will deposit more energy in the calorimeters. At the LHC, a muon mostly loses its energy by ioniza-

⁵ We assume LLCPs are produced by large energy transfer, which results in smaller $|\eta|$ of the LLCPs.

TABLE II: Contributions to SRs in the 14 TeV LHC analysis with efficiency factors (ϵ_μ and $\epsilon_{\tilde{\tau}}$) included, and 95% CL upper limits on the number of events (N_{UL}) for integrated luminosities $\int \mathcal{L} = 0.1, 0.3, \text{ and } 3 \text{ ab}^{-1}$, based on \tilde{e}_L production ($N_{\text{gen;LL}} = 1$). Statistical uncertainties are considered but systematic uncertainties are not included. In the columns of signal event contributions, bold numbers mark the SR which gives the lowest CL_s in the analysis of $\int \mathcal{L} = 0.3 \text{ ab}^{-1}$, and contributions less than 0.1 ab are displayed as zero.

	signal ($pp \rightarrow \tilde{e}_L \tilde{e}_L^*$) [ab] with $m_{\tilde{e}_L} =$				SM BKG [ab]	N_{UL} with $\int \mathcal{L} =$		
	400 GeV	600 GeV	800 GeV	1 TeV		0.1 ab^{-1}	0.3 ab^{-1}	3 ab^{-1}
$N_{\text{LLCP}} = 2$	262	50	12	3.5	323	—	—	—
SR300	259	50	12	3.5	2.8	3.4	4.0	7.5
SR400	74	50	12	3.5	0.67	3.1	3.3	4.9
SR500	0.85	47	12	3.5	0.19	3.0	3.1	3.8
SR600	0	13	12	3.5	6×10^{-2}	3.0	3.0	3.3
SR700	0	0.28	11	3.5	2×10^{-2}	3.0	3.0	3.1
SR800	0	0	3.1	3.4	6×10^{-3}	3.0	3.0	3.0
SR900	0	0	0	3.0	2×10^{-3}	3.0	3.0	3.0
SR1000	0	0	0	0.86	$< 10^{-3}$	3.0	3.0	3.0

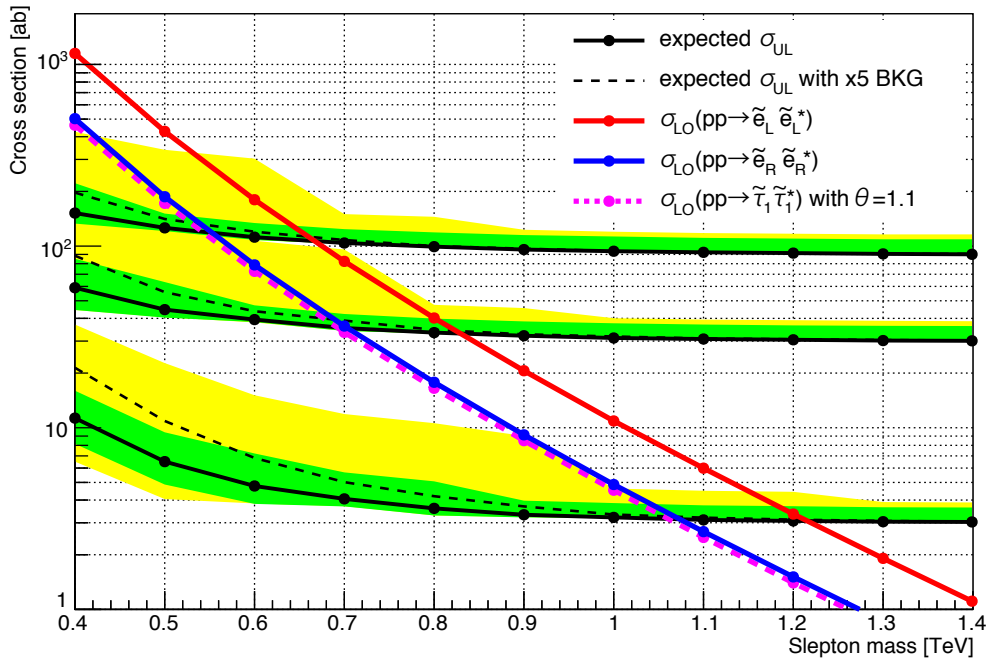


FIG. 2: Summary plot of the potential reach of LLCP searches at the 14 TeV LHC. The thick black lines give the expected upper limits σ_{UL} on the signal cross section for integrated luminosities $\int \mathcal{L} = 0.1, 0.3, \text{ and } 3 \text{ ab}^{-1}$ from top to bottom. Green (yellow) bands show the 68% (95%) statistical uncertainty regions of σ_{UL} . To estimate the effect of systematic uncertainty on the background, the expected σ_{UL} assuming a five-times larger background is also shown (black dashed lines). Signal cross sections are calculated at tree-level and drawn as red, blue, and magenta solid lines, assuming Drell–Yan pair production of $\tilde{e}_L \tilde{e}_L^*$, $\tilde{e}_R \tilde{e}_R^*$, and $\tilde{\tau}_1 \tilde{\tau}_1^*$ with the stau mixing angle $\theta = 1.1$, respectively.

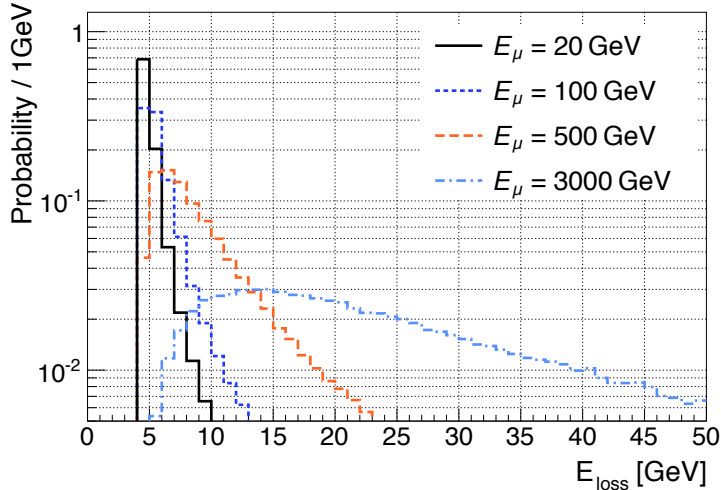


FIG. 3: Energy loss of muons in 3 m iron. Note that this includes the ionization energy loss of 4.8 (6.0) GeV for $E_\mu = 20$ (3000) GeV.

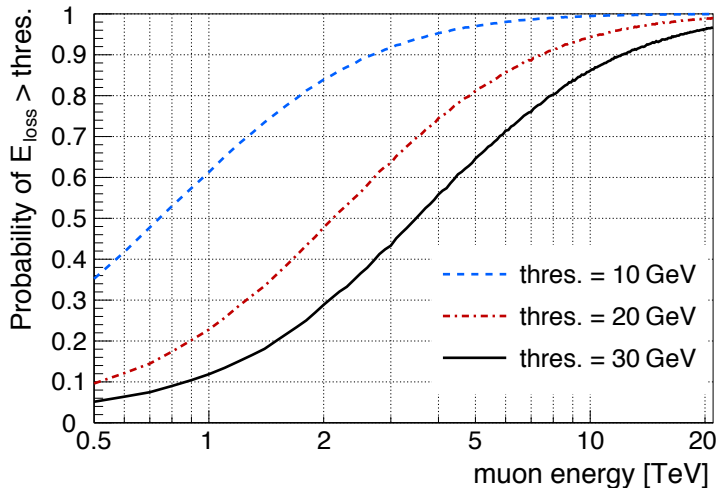


FIG. 4: The probability that the energy loss of a muon in a detector exceeds certain thresholds as a function of the muon energy. The detector is modeled as 3 m of iron.

tion [20]⁶. In iron, the ionization energy loss is 1.6–2.0 GeV/m for $E_\mu = 20$ –3000 GeV. However, energetic muons can additionally lose energy through radiative processes. We use `Geant 4.10` [38] to estimate this effect. Figure 3 illustrates the total energy loss of muons in a hypothetical 3 m-thick iron detector. For $E_\mu \geq 500$ GeV, the energy loss is significant. The probability that the energy loss exceeds 10, 20 or 30 GeV is shown in Fig. 4.

Second, the P_T resolution of muons is expected to be worse. In general, the P_T resolution in trackers can be parametrized as

$$\Delta P_T = A \oplus B \cdot P_T \oplus C \cdot P_T^2, \quad (15)$$

⁶ See also Ref. [37, Sec. 32]

where the contribution to A is due to muon energy loss before the tracker, B comes from multiple scattering, and C from the resolution of position measurements. For high- P_T , the resolution is therefore dominated by the P_T^2 term [39] (see also Ref. [40]),

$$\Delta P_T \approx C \cdot P_T^2. \quad (16)$$

In our analysis for the 14 TeV LHC, the muon P_T resolution was approximated as $\Delta P_T = 0.05 P_T$. This should be supplemented by the effect of C in analyses of 100 TeV collisions. The value of C was measured by ATLAS at a very early stage of the 7 TeV run to be $C = 0.168(16) \text{ TeV}^{-1}$ and $0.417(11) \text{ TeV}^{-1}$ for the barrel region of the MS and ID, respectively [39]. Since stronger magnetic fields in the tracker, as well as larger detector dimensions, would improve the momentum resolution, we use $C = 0.1 \text{ TeV}^{-1}$ in the following analysis⁷.

2. Method

Our discussion here closely follows the discussion of Sec. III A, with the two novel aspects being the worse momentum resolution and muon radiative energy loss discussed above. As before, slepton pair production is calculated using `MadGraph5_aMC@NLO` [31] at tree-level, with showering and hadronization performed by `Pythia 6` [32] with the `Pythia-PGS` interface. The Snowmass background set for 100 TeV colliders is used for the SM background events, with the detector assumed to be as described in Sec. III B. Pileup is not considered.

In the Snowmass background set, and thus in the `Delphes` detector simulation in our signal event generation, muon momenta (for $|\eta| < 2.5$ and $P_T > 200 \text{ GeV}$) are smeared according to $\Delta P_T = 0.05 P_T$. We think this is too optimistic for $P_T \gtrsim 500 \text{ GeV}$, and exploit “momentum re-smearing” in object identification.

Object identification and event selection are implemented as follows. First, after object identification by `Delphes`, all objects with $P_T < 100 \text{ GeV}$ are dropped. Then, the momenta of the remaining muons are re-smearred according to the normal distribution

$$N(P_T, C \cdot P_T^2), \quad (17)$$

where $C = 0.1 \text{ TeV}^{-1}$, and P_T is the momentum after the `Delphes` detector simulation. After that, muon pairs are removed if their invariant masses satisfy $|m_{\mu\mu} - m_Z| < 5 \text{ GeV}$.

For further suppression of background muons, we exploit the muon radiative energy loss. Because the background for $m_{\tilde{l}} \sim 1 \text{ TeV}$ sleptons under our event selection is from energetic muons with $P_T \gtrsim 500 \text{ GeV}$, we can reduce the number of background events by requiring the energy loss of a candidate LLCP to be below a certain threshold. The measured energy loss, E_{loss} , is the sum of the energy deposits along the candidate’s trajectory in the calorimeter (corrected for pile-up). We note that, while they do not have radiative energy loss, true LLCPs have larger energy deposits from ionization compared to minimum ionizing particles of the same momentum, because of their smaller $\beta\gamma$. For $m = 0.4$ to 3 TeV sleptons, the

⁷ This discussion can be easily understood by approximating the momentum measurement as a sagitta measurement. When a particle of charge q and momentum \mathbf{p} flies a distance L in a magnetic field B , it has sagitta $s = qL^2B/8p_{\perp}$, where p_{\perp} is the component of \mathbf{p} perpendicular to \mathbf{B} . Assuming that the uncertainty of the sagitta measurement is a constant Δs , the uncertainty of p_{\perp} is $\Delta p_{\perp} \simeq 8p_{\perp}^2 \Delta s / qL^2B$.

TABLE III: LLCP selection flow and cross section of events in the 100 TeV pp collider analysis, where efficiencies ϵ_μ and $\epsilon_{\tilde{\tau}}$ are not included, for the case with \tilde{e}_L pair-production ($N_{\text{gen;LL}} = 1$). The same conventions as in Table I are used.

	signal ($pp \rightarrow \tilde{e}_L \tilde{e}_L^*$) with $m_{\tilde{e}_L} =$				SM BKG
	1 TeV	2 TeV	3 TeV	4 TeV	—
LLCP selection flow [ab]					
candidates	2.57×10^3	179	31.8	8.27	—
+ $P_T > 500$ GeV, isolated	1.84×10^3	153	28.5	7.49	9.19×10^6
+ $0.4 < \hat{\beta} < 0.95$	1.23×10^3	121	24.6	6.83	3.41×10^5
+ $E_{\text{loss}} < 30$ GeV	—	—	—	—	2.78×10^5
Event cross section [ab]					
total cross section	1.28×10^3	89.5	15.9	4.14	—
$N_{\text{LLCP}} = 1$	378	27.8	4.46	1.03	2.78×10^5
$N_{\text{LLCP}} = 2$	424	46.5	10.1	2.90	34.6

energy loss in 3 m of iron is estimated as $E_{\text{loss}} = 21.7, 13.4,$ and 9.20 GeV for $\beta = 0.3, 0.4,$ and $0.5,$ respectively. Obviously, the details of detector response and energy resolution will depend on the actual detector design. Here we require LLCPs to have $\hat{\beta} > 0.4$ and $E_{\text{loss}} < 30$ GeV, and assume that a true (slepton) LLCP always satisfies the latter condition⁸. The β resolution is modeled in the same way as in the 14 TeV analysis. Accordingly, any remaining muon is tagged as an LLCP if it satisfies the following conditions:

- $P_T > 500$ GeV and $|\eta| < 2.4,$
- $\Delta R > 0.5$ from the nearest reconstructed object (with $P_T > 100$ GeV),
- $0.4 < \hat{\beta} < 0.95,$
- $E_{\text{loss}} < 30$ GeV.

Events containing two LLCP candidates are selected, and SRs are defined in the same manner as in Sec. III A, with 16 SRs: SR500, SR600, ..., and SR2000. The efficiencies $\epsilon_\mu = 0.5$ and $\epsilon_{\tilde{\tau}} = 0.6$ are also imposed. Statistical uncertainties are considered, but systematic uncertainties are not included.

3. Results

The selection flow is presented in Table III, with the cross section broken into different signal regions in Table IV. The efficiency factors ϵ_μ and $\epsilon_{\tilde{\tau}}$, are included in Table IV but not in Table III.

In Fig. 5, we show the resulting limits for different scenarios. The efficiency factors ϵ_μ and $\epsilon_{\tilde{\tau}}$, are taken into account in this plot. The upper bound σ_{UL} on the signal cross section

⁸ The reduction of signal events due to the tighter β cut is negligible (less than 2%).

TABLE IV: Contributions to SRs in the 100 TeV pp collider analysis with efficiency factors (ϵ_μ and $\epsilon_{\tilde{\tau}}$) included, and 95% CL upper limits on the number of events (N_{UL}) for integrated luminosities $\int \mathcal{L} = 0.3, 1, \text{ and } 3 \text{ ab}^{-1}$, based on \tilde{e}_L pair-production ($N_{\text{gen;LL}} = 1$). Not all SRs are shown. Statistical uncertainties are considered, but systematic uncertainties are not included. Bold numbers mark the SRs that give the lowest CL_s in the analysis of $\int \mathcal{L} = 1 \text{ ab}^{-1}$.

	signal ($pp \rightarrow \tilde{e}_L \tilde{e}_L^*$) [ab] with $m_{\tilde{e}_L} =$				SM BKG [ab]	N_{UL} with $\int \mathcal{L} =$		
	1 TeV	2 TeV	3 TeV	4 TeV		0.3 ab^{-1}	1 ab^{-1}	3 ab^{-1}
$N_{\text{LLCP}} = 2$	153	17	3.6	1.0	8.7	—	—	—
SR500	152	17	3.6	1.0	1.6	3.6	4.1	6.2
SR700	146	17	3.6	1.0	0.61	3.3	3.5	4.7
SR1000	43	16	3.5	1.0	0.14	3.1	3.1	3.6
SR1200	4.0	16	3.5	1.0	0.06	3.0	3.1	3.3
SR1500	0.33	13	3.3	0.97	0.03	3.0	3.0	3.1
SR1700	0.10	10	3.2	0.94	0.007	3.0	3.0	3.0
SR2000	0	4.4	2.9	0.90	0.003	3.0	3.0	3.0

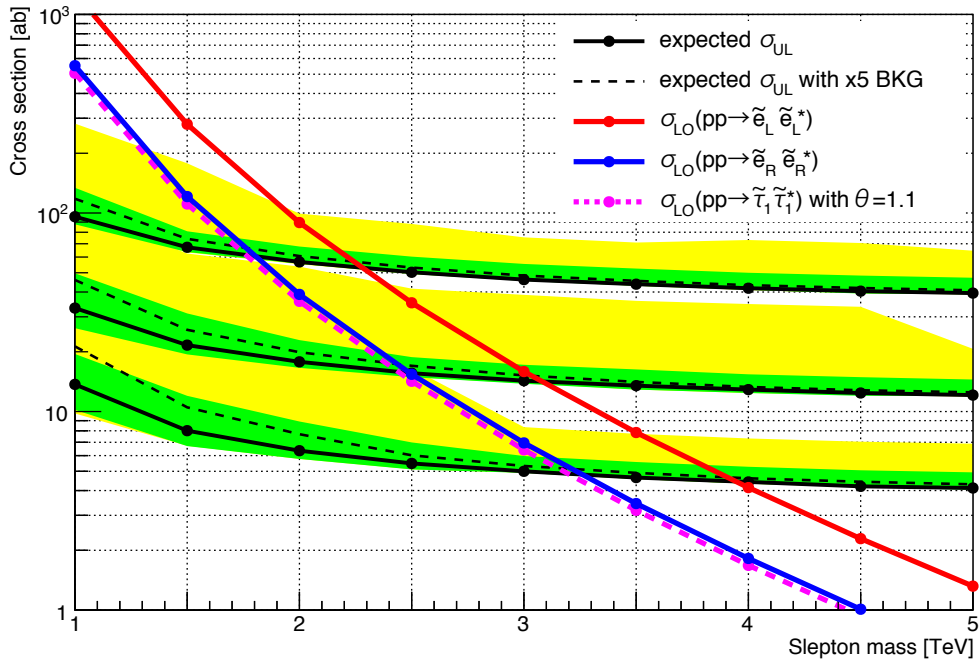


FIG. 5: As in Fig. 2, but for a 100 TeV pp collider. The upper limits on the signal cross section (black solid lines with statistical uncertainty bands) are for integrated luminosities of $\int \mathcal{L} = 0.3, 1, \text{ and } 3 \text{ ab}^{-1}$ from top to bottom.

TABLE V: Expected mass limits of long-lived sleptons at the 14 TeV LHC and future 100 TeV pp colliders, based on the analysis described in Secs. III A and III B; i.e., long-lived sleptons below these bounds are expected to be excluded at 95% CL if no excess is observed. Left-handed (right-handed) sleptons correspond to left-right mixing angles of $\theta = 0$ ($\pi/2$), and “least production” is for the minimal signal cross section at $\theta = 1.1$. For $N_{\text{gen;LL}} = 3$, all sleptons are assumed to have the same mass and mixing angle.

	14 TeV LHC			100 TeV pp collider		
	0.1 ab ⁻¹	0.3 ab ⁻¹	3 ab ⁻¹	0.3 ab ⁻¹	1 ab ⁻¹	3 ab ⁻¹
$N_{\text{gen;LL}} = 1$, left-handed	0.66 TeV	0.83 TeV	1.21 TeV	2.28 TeV	3.08 TeV	3.95 TeV
$N_{\text{gen;LL}} = 1$, right-handed	0.55 TeV	0.70 TeV	1.07 TeV	1.81 TeV	2.49 TeV	3.25 TeV
$N_{\text{gen;LL}} = 1$, least production	0.54 TeV	0.69 TeV	1.06 TeV	1.76 TeV	2.44 TeV	3.20 TeV
$N_{\text{gen;LL}} = 3$, all left-handed	0.83 TeV	1.01 TeV	1.41 TeV	3.02 TeV	3.97 TeV	4.96 TeV
$N_{\text{gen;LL}} = 3$, all right-handed	0.70 TeV	0.88 TeV	1.27 TeV	2.45 TeV	3.30 TeV	4.20 TeV

is computed for $\int \mathcal{L} = 0.3, 1$, and 3 ab^{-1} and is shown as black solid lines. The effect of statistical and systematic uncertainties are displayed by the bands and the black dashed lines, respectively (see Fig. 2). The red (blue) line gives the production cross section for a left- (right-) handed slepton, and the magenta line corresponds to a slepton with a mixing angle of $\theta = 1.1$, which minimizes the production cross section.

IV. DISCUSSION

The results of our analysis are collected in Table V, where we show the expected sensitivity of the 14 TeV LHC and 100 TeV collider. The various entries show the lower bounds on long-lived sleptons, assuming that the obtained data is consistent with the SM expectation. The first three lines of the table are based on pair production of a single slepton type and denoted by $N_{\text{gen;LL}} = 1$. The last two lines, with $N_{\text{gen;LL}} = 3$, assume three degenerate long-lived sleptons, which are either left-handed or right-handed, so that the production cross sections are a factor of three larger.

It is instructive to interpret these results in terms of the integrated luminosity required for excluding long-lived sleptons of a particular mass. This is shown in Fig. 6 for the case $N_{\text{gen;LL}} = 1$ for $\theta = 0, \pi/2$ and 1.1 . For different values of $N_{\text{gen;LL}}$, the required luminosity is a factor of $N_{\text{gen;LL}}$ smaller.

In the same manner, discovery sensitivity, i.e., the luminosity required for 3σ -evidence and 5σ -discovery, is illustrated in Fig. 7. Here, the 5σ -level (3σ -level) signature in one-sided tests is defined as having the p -value of the background-only hypothesis smaller than 2.9×10^{-7} (0.0013).

If an LLCP is discovered, the resolution of its mass determination will be of great interest. Figs. 8 and 9 display the reconstructed mass of LLCP candidates in selected events. As the slepton mass m_{LLCP} increases, the cross section decreases and with it the number of true LLCPs produced. At the same time, because \hat{m} peaks near m_{LLCP} , the background contribution under the peak falls sharply, and the \hat{m} distribution in this region is virtually background free. It is for this reason that the expected σ_{UL} in Figs. 2 and 5 is nearly flat for larger m_{LLCP} .

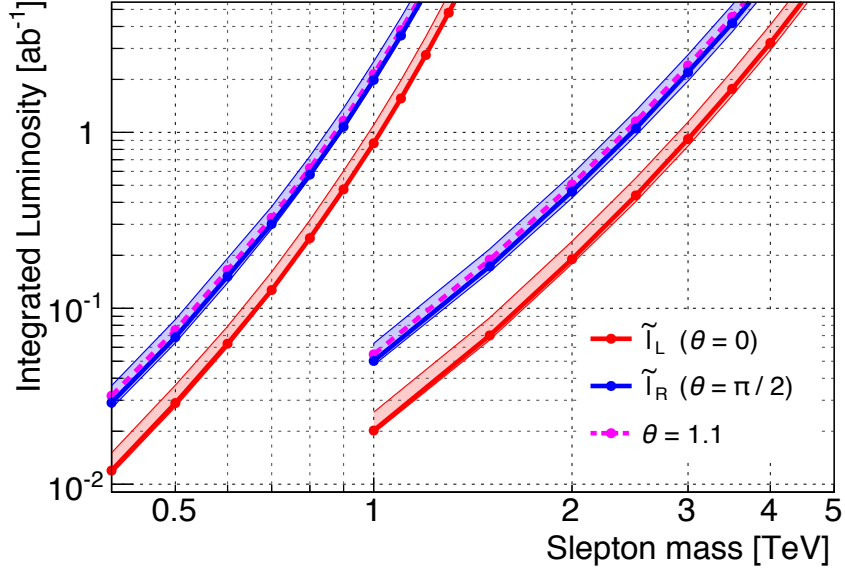


FIG. 6: The integrated luminosity required for excluding long-lived sleptons at 95% CL for $N_{\text{gen;LL}} = 1$ for three values of the slepton left–right mixing angle θ . For each θ , the left-hand (right-hand) contour shows the required integrated luminosity for the 14 TeV LHC (future 100 TeV pp collider). The lines for $\theta = 0$ and $\pi/2$ are drawn as bands, which show the 68% statistical uncertainty of the expectation.

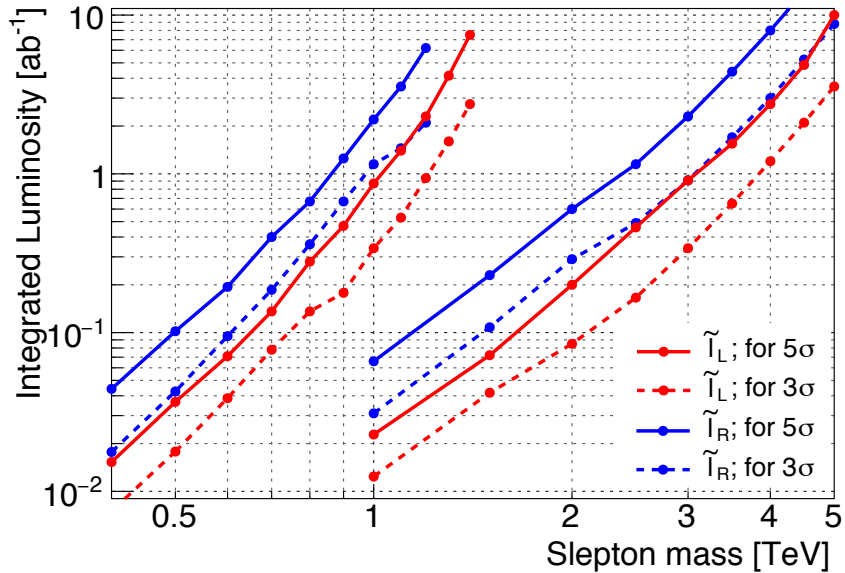


FIG. 7: The same as Fig. 6, but for the discovery of long-lived sleptons. Solid (dashed) lines are for 5σ - (3σ -)discoveries.

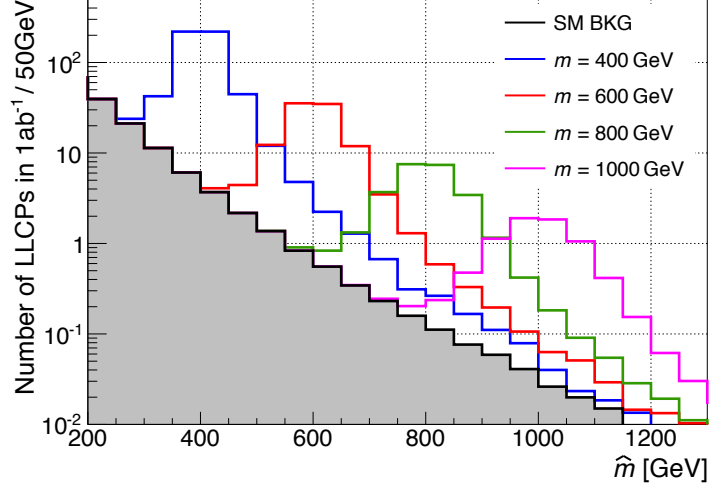


FIG. 8: Distribution of the reconstructed LLCP mass \hat{m} in the 14 TeV LHC analysis (Sec. III A). The gray region is the contribution from SM background muons, on which signal contributions are stacked. Note that this shows the number of particles, not of events.

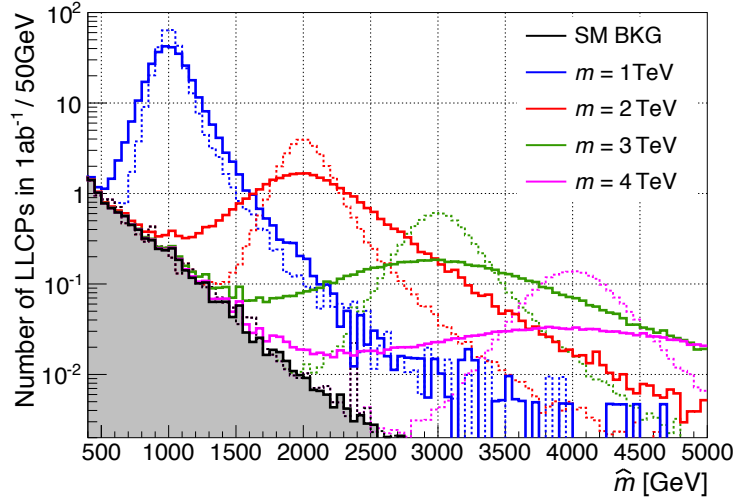


FIG. 9: As in Fig. 8, but for the 100 TeV pp collider analysis (Sec. III B). Solid lines are for the nominal analysis with $C = 0.1 \text{ TeV}^{-1}$, and dotted lines show the result without momentum re-smearing, i.e., with $C = 0$.

A key ingredient in the mass measurement is the resolution of the momentum measurement, which typically deteriorates for large P_T . In Fig. 9, we examine the effect of the P_T^2 term of Eq. (15) on the mass measurement. In addition to the solid lines obtained as described above with $C = 0.1 \text{ TeV}^{-1}$, we show the results obtained with $C = 0$ as dotted lines. Even with $C = 0$, the peaks are softer for larger values of the mass because the momentum resolution scales as $\Delta P_T = 0.05 P_T$. With non-zero C , the resolution clearly deteriorates for $m_{\text{LLCP}} = 3\text{--}4 \text{ TeV}$. Thus, momentum resolution is crucial for the discovery of LLCs with masses $\gtrsim 3 \text{ TeV}$. It is also notable that the background distribution (dotted black line) is hardly affected by this factor, since it essentially cuts off below 3 TeV .

Pile-up events are not included in this analysis, because the LLC searches focus on particles with very large momenta. Pile-up events tend to produce less energetic particles, so their effects on the P_T or β measurements of very energetic particles should be small. On the other hand, pile-up may worsen the resolution of the E_{loss} measurement, which we used to reduce background. This issue is related to lepton identification, and it should be carefully examined in future studies on detector design.

For the 100 TeV analysis, we required E_{loss} below 30 GeV , since the typical energy loss of $\beta = 0.4$ sleptons is around 13 GeV . The E_{loss} cut reduces 18% of fake LLCs (cf. Table III), which ultimately reduces the background events by 34%, because signal events are required to have two LLCs. If the energy resolution in the calorimeters is better than assumed here, a tighter cut on E_{loss} could be used. On the other hand, pile-up events may worsen the energy resolution.

V. CONCLUSIONS

We have discussed the prospects for LLC searches at the 14 TeV LHC and at a 100 TeV pp collider. We use sleptons as the benchmark LLC, with Drell–Yan slepton-pair production as the sole slepton production channel.

For scenarios in which only a single type of long-lived slepton is produced ($N_{\text{gen;LL}} = 1$), the 14 TeV LHC is expected to constrain the LLC mass as $m_{\text{LLCP}} > 700\text{--}800 \text{ GeV}$ with 0.3 ab^{-1} , and $1.1\text{--}1.2 \text{ TeV}$ with 3 ab^{-1} , depending on the amount of left–right slepton mixing. Thus, the entire parameter space of the slepton–neutralino co-annihilation scenario can be probed at the LHC. At a 100 TeV pp collider, the sensitivity is expected to reach $1.8\text{--}2.3 \text{ TeV}$ for 0.3 ab^{-1} , and $3.2\text{--}4.0 \text{ TeV}$ for 3 ab^{-1} . In terms of discovery, the 14 TeV LHC is expected to discover $600\text{--}800 \text{ GeV}$ ($1.0\text{--}1.2 \text{ TeV}$) long-lived sleptons with 0.3 ab^{-1} (3 ab^{-1}), while a 100 TeV collider’s coverage is estimated to slepton masses up to $1.6\text{--}2.2 \text{ TeV}$ ($3.1\text{--}4.1 \text{ TeV}$) with 0.3 ab^{-1} (3 ab^{-1}).

We have found that, in 100 TeV proton collisions, the radiative energy loss of energetic muons is significant. We exploited this fact to reject fake LLCs coming from SM muons. On the other hand, the momentum resolution, which plays a key role in the LLC mass measurement, will be more challenging at a high-energy collider. This effect is clearly seen in Fig. 9. The momentum resolution can be improved by increasing the magnetic field strength as well as by using a bigger tracker. Since momentum measurements are essential for any searches at collider experiments, detailed studies of the required resolution and the implications for detector design are critical.

Acknowledgments

J.L.F. and Y.S. thank the CERN Theoretical Physics Group and J.L.F. thanks the Technion Center for Particle Physics for hospitality. The work of J.L.F. and Y.S. is supported in part by BSF Grant No. 2010221. The work of J.L.F. is also supported in part by NSF Grant No. PHY-1316792 and by a Guggenheim Foundation grant. The research of Y.S., S.I., and S.T. is also supported by the ICORE Program of Planning and Budgeting Committee, and by ISF Grant Nos. 1937/12 (Y.S. and S.I.) and 1787/11 (S.T.).

Appendix A: Detailed Description of the Monte Carlo Simulation

1. Background Events

We use the Snowmass backgrounds for pp colliders with $\sqrt{s} = 14$ and 100 TeV [28–30] as the SM background contributions. These backgrounds are available with and without pile-up; for simplicity, we used the backgrounds without pile-up. Here we review the procedure used to generate the Snowmass background.

The backgrounds were generated with `MadGraph5` [41], together with `BRIDGE` [42]. `Pythia6.4` [32] was used for parton showering and hadronization with the `Pythia-PGS` interface, and `Delphes`, tuned by the Snowmass Collaboration based on `Delphes3.0.9` [33–35], was used for detector simulation, with jet reconstruction implemented with `FastJet` [34, 35].

The detector simulation of the background events, which is summarized in Ref. [28]⁹, is based on a detector which has a tracker, an electromagnetic and a hadronic calorimeter. Tracking efficiency and resolution in the tracker, and energy resolution in the calorimeters are included. The energy flow method is utilized for calorimeter analysis.

Electrons (e^\pm) and muons (μ^\pm) are reconstructed from an isolated track originating from true electrons and true muons, respectively, where a charged-particle track is called isolated if the scalar sum of P_T of tracks and calorimeter hits around the track ($\Delta R < 0.3$) is less than 10% of the track P_T . Electrons (muons) must satisfy $P_T > 10$ GeV and $|\eta| < 2.5$ (2.4). Lepton momentum is smeared with a tracker resolution, which for muons with $P_T > 200$ GeV is set to $\Delta P_T = 0.05 P_T$. Note that the information from the calorimeters is not used here, and that misidentifications are not considered.

Jets are reconstructed by the anti- k_T algorithm with $\Delta R = 0.5$ using the `FastJet` package. A calorimeter cluster is identified as a photon if the cluster has hits from photons or e^\pm 's and μ^\pm 's, but is not associated with any reconstructed track. Otherwise the cluster is identified as a jet. The missing energy (\cancel{E}_T) is calculated from the reconstructed tracks and calorimeter hits.

2. Signal Events

Signal events are generated following the procedure of Snowmass background generation. `Madgraph5` [31] is used as the event generator, and `Pythia6.428` and `Delphes` are used

⁹ The parameters are slightly modified: `Radius` in `ParticlePropagator` is set to 1.29 m, and the muon tracking efficiency is set to 99.98% for $|\eta| < 1.5$ and 98.0% for $1.5 < |\eta| < 2.5$.

with the same parameters used to generate the Snowmass background.

The long-lived sleptons are treated as stable particles. They are reconstructed as muons (μ^\pm) if they have velocity $\beta > 0.3$, $P_T > 10$ GeV and $|\eta| < 2.4$; otherwise they are ignored.

3. Momentum Re-smearing

As discussed in Sec. III B, momentum resolution deteriorates at very high momentum, because the trajectory becomes straighter for large P_T . For very large P_T , the momentum resolution is approximated as $\Delta P_T \propto P_T^2$. This effect is important for a 100 TeV collider, but it has not yet been modeled in the procedure described above. Therefore, for the 100 TeV collider simulation we smeared the reconstructed momentum of charged tracks again with the distribution $N(P_T, CP_T^2)$, with $C = 0.1 \text{ TeV}^{-1}$. In the 14 TeV simulation, this re-smearing was not employed.

4. Object Selection

The background events provided by the Snowmass collaboration and the generated signal events are then subjected to further object selections. First, all objects with $P_T < 100$ GeV in the 100 TeV analysis, and with $P_T < 30$ GeV in the 14 TeV analysis, are removed. Electrons, jets, and photons are required to have $|\eta| < 2.5$, and muons are required to have $|\eta| < 2.4$. Muon pairs are removed if their invariant masses satisfy $|m_{\mu\mu} - m_Z| < 5$ GeV.

Then, a ‘‘muon’’ is regarded as a LLCP if it satisfies the following conditions:

- $\Delta R > 0.5$ from the nearest objects (electrons, muons, jets, and photons)
- In the 14 TeV analysis, $\hat{P}_T > 100$ GeV, $|\eta| < 2.4$, and $0.3 < \hat{\beta} < 0.95$
- In the 100 TeV analysis, $\hat{P}_T > 500$ GeV, $|\eta| < 2.4$, and $0.4 < \hat{\beta} < 0.95$
- In the 100 TeV analysis, $E_{\text{loss}} < 30$ GeV .

In the conditions above, $\hat{\beta}$ is the smeared velocity, which obeys the following distributions

$$\text{PDF}(\hat{\beta})_\mu = 0.832 N(1, 0.022) + 0.162 N(1, 0.050) + 0.00534 N(1, 0.116), \quad (\text{A1})$$

$$\text{PDF}(\hat{\beta}^{-1})_{\tilde{l}} = N(\beta^{-1}, 0.025), \quad (\text{A2})$$

for background muons and signal sleptons, respectively. E_{loss} is the energy deposit of the particles in the calorimeter. For muons, it is simulated with **Geant 4.10** [38], where the calorimeter is approximated as 3.0 m iron. Sleptons are assumed to pass this cut because the energy loss is far less than the threshold (see Sec. III B).

After these object identifications, events are selected and analyzed as summarized in Secs. III A and III B.

[1] CMS Collaboration, S. Chatrchyan *et al.*, ‘‘Searches for long-lived charged particles in pp collisions at $\sqrt{s}=7$ and 8 TeV,’’ *JHEP* **1307** (2013) 122, [arXiv:1305.0491](https://arxiv.org/abs/1305.0491) [hep-ex].

- [2] **ATLAS** Collaboration, G. Aad *et al.*, “Searches for heavy long-lived charged particles with the ATLAS detector in proton-proton collisions at $\sqrt{s} = 8$ TeV,” [arXiv:1411.6795 \[hep-ex\]](#).
- [3] **CMS** Collaboration, V. Khachatryan *et al.*, “Constraints on the pMSSM, AMSB model and on other models from the search for long-lived charged particles in proton-proton collisions at $\sqrt{s} = 8$ TeV,” [arXiv:1502.02522 \[hep-ex\]](#).
- [4] Y. Gershtein, M. Luty, M. Narain, L. T. Wang, D. Whiteson, *et al.*, “Working Group Report: New Particles, Forces, and Dimensions,” [arXiv:1311.0299 \[hep-ex\]](#).
- [5] M. Low and L.-T. Wang, “Neutralino dark matter at 14 TeV and 100 TeV,” *JHEP* **1408** (2014) 161, [arXiv:1404.0682 \[hep-ph\]](#).
- [6] B. S. Acharya, K. Bozek, C. Pongkitivanichkul, and K. Sakurai, “Prospects for observing charginos and neutralinos at a 100 TeV proton-proton collider,” [arXiv:1410.1532 \[hep-ph\]](#).
- [7] S. Gori, S. Jung, L.-T. Wang, and J. D. Wells, “Prospects for Electroweakino Discovery at a 100 TeV Hadron Collider,” *JHEP* **1412** (2014) 108, [arXiv:1410.6287 \[hep-ph\]](#).
- [8] M. Dine, A. E. Nelson, and Y. Shirman, “Low-energy dynamical supersymmetry breaking simplified,” *Phys.Rev.* **D51** (1995) 1362–1370, [arXiv:hep-ph/9408384 \[hep-ph\]](#).
- [9] M. Dine, A. E. Nelson, Y. Nir, and Y. Shirman, “New tools for low-energy dynamical supersymmetry breaking,” *Phys.Rev.* **D53** (1996) 2658–2669, [arXiv:hep-ph/9507378 \[hep-ph\]](#).
- [10] J. L. Feng and T. Moroi, “Tevatron signatures of longlived charged sleptons in gauge mediated supersymmetry breaking models,” *Phys.Rev.* **D58** (1998) 035001, [arXiv:hep-ph/9712499 \[hep-ph\]](#).
- [11] T. Cohen, T. Golling, M. Hance, A. Henrichs, K. Howe, *et al.*, “SUSY Simplified Models at 14, 33, and 100 TeV Proton Colliders,” *JHEP* **1404** (2014) 117, [arXiv:1311.6480 \[hep-ph\]](#).
- [12] J. L. Feng, A. Rajaraman, and F. Takayama, “Superweakly interacting massive particles,” *Phys.Rev.Lett.* **91** (2003) 011302, [arXiv:hep-ph/0302215 \[hep-ph\]](#).
- [13] J. L. Feng, A. Rajaraman, and F. Takayama, “SuperWIMP dark matter signals from the early universe,” *Phys.Rev.* **D68** (2003) 063504, [arXiv:hep-ph/0306024 \[hep-ph\]](#).
- [14] K. Griest and D. Seckel, “Three exceptions in the calculation of relic abundances,” *Phys.Rev.* **D43** (1991) 3191–3203.
- [15] J. R. Ellis, T. Falk, and K. A. Olive, “Neutralino - Stau coannihilation and the cosmological upper limit on the mass of the lightest supersymmetric particle,” *Phys.Lett.* **B444** (1998) 367–372, [arXiv:hep-ph/9810360 \[hep-ph\]](#).
- [16] Y. Konishi, S. Ohta, J. Sato, T. Shimomura, K. Sugai, *et al.*, “First evidence of the constrained minimal supersymmetric standard model is appearing soon,” *Phys.Rev.* **D89** no. 7, (2014) 075006, [arXiv:1309.2067 \[hep-ph\]](#).
- [17] N. Desai, J. Ellis, F. Luo, and J. Marrouche, “Closing in on the Tip of the CMSSM Stau Coannihilation Strip,” [arXiv:1404.5061 \[hep-ph\]](#).
- [18] J. Heisig and J. Kersten, “Production of long-lived staus in the Drell-Yan process,” *Phys.Rev.* **D84** (2011) 115009, [arXiv:1106.0764 \[hep-ph\]](#).
- [19] J. Heisig and J. Kersten, “Long-lived staus from strong production in a simplified model approach,” *Phys.Rev.* **D86** (2012) 055020, [arXiv:1203.1581 \[hep-ph\]](#).
- [20] D. E. Groom, N. V. Mokhov, and S. I. Striganov, “Muon stopping power and range tables 10-MeV to 100-TeV,” *Atom.Data Nucl.Data Tabl.* **78** (2001) 183–356.

- [21] J. L. Feng, S. Su, and F. Takayama, “Supergravity with a gravitino LSP,” *Phys.Rev.* **D70** (2004) 075019, [arXiv:hep-ph/0404231 \[hep-ph\]](#).
- [22] J. Bernstein, L. S. Brown, and G. Feinberg, “The Cosmological Heavy Neutrino Problem Revisited,” *Phys.Rev.* **D32** (1985) 3261.
- [23] R. J. Scherrer and M. S. Turner, “On the Relic, Cosmic Abundance of Stable Weakly Interacting Massive Particles,” *Phys.Rev.* **D33** (1986) 1585.
- [24] T. Asaka, K. Hamaguchi, and K. Suzuki, “Cosmological gravitino problem in gauge mediated supersymmetry breaking models,” *Phys.Lett.* **B490** (2000) 136–146, [arXiv:hep-ph/0005136 \[hep-ph\]](#).
- [25] J. L. Feng, S.-f. Su, and F. Takayama, “SuperWIMP gravitino dark matter from slepton and sneutrino decays,” *Phys.Rev.* **D70** (2004) 063514, [arXiv:hep-ph/0404198 \[hep-ph\]](#).
- [26] M. Kawasaki, K. Kohri, T. Moroi, and A. Yotsuyanagi, “Big-Bang Nucleosynthesis and Gravitino,” *Phys.Rev.* **D78** (2008) 065011, [arXiv:0804.3745 \[hep-ph\]](#).
- [27] S. Bailly, K. Jedamzik, and G. Moulhaka, “Gravitino Dark Matter and the Cosmic Lithium Abundances,” *Phys.Rev.* **D80** (2009) 063509, [arXiv:0812.0788 \[hep-ph\]](#).
- [28] J. Anderson, A. Avetisyan, R. Brock, S. Chekanov, T. Cohen, *et al.*, “Snowmass Energy Frontier Simulations,” [arXiv:1309.1057 \[hep-ex\]](#).
- [29] A. Avetisyan, J. M. Campbell, T. Cohen, N. Dhirga, J. Hirschauer, *et al.*, “Methods and Results for Standard Model Event Generation at $\sqrt{s} = 14$ TeV, 33 TeV and 100 TeV Proton Colliders (A Snowmass Whitepaper),” [arXiv:1308.1636 \[hep-ex\]](#).
- [30] A. Avetisyan, S. Bhattacharya, M. Narain, S. Padhi, J. Hirschauer, *et al.*, “Snowmass Energy Frontier Simulations using the Open Science Grid (A Snowmass 2013 whitepaper),” [arXiv:1308.0843 \[hep-ex\]](#).
- [31] J. Alwall, R. Frederix, S. Frixione, V. Hirschi, F. Maltoni, *et al.*, “The automated computation of tree-level and next-to-leading order differential cross sections, and their matching to parton shower simulations,” *JHEP* **1407** (2014) 079, [arXiv:1405.0301 \[hep-ph\]](#).
- [32] T. Sjostrand, S. Mrenna, and P. Z. Skands, “PYTHIA 6.4 Physics and Manual,” *JHEP* **05** (2006) 026, [arXiv:hep-ph/0603175](#). <http://arxiv.org/abs/hep-ph/0603175>.
- [33] **DELPHES 3** Collaboration, J. de Favereau *et al.*, “DELPHES 3, A modular framework for fast simulation of a generic collider experiment,” *JHEP* **1402** (2014) 057, [arXiv:1307.6346 \[hep-ex\]](#).
- [34] M. Cacciari, G. P. Salam, and G. Soyez, “FastJet User Manual,” *Eur.Phys.J.* **C72** (2012) 1896, [arXiv:1111.6097 \[hep-ph\]](#).
- [35] M. Cacciari and G. P. Salam, “Dispelling the N^3 myth for the k_t jet-finder,” *Phys.Lett.* **B641** (2006) 57–61, [arXiv:hep-ph/0512210 \[hep-ph\]](#).
- [36] A. L. Read, “Presentation of search results: The CL(s) technique,” *J.Phys.* **G28** (2002) 2693–2704.
- [37] **Particle Data Group** Collaboration, K. Olive *et al.*, “Review of Particle Physics,” *Chin.Phys.* **C38** (2014) 090001.
- [38] **GEANT4** Collaboration, S. Agostinelli *et al.*, “GEANT4: A Simulation toolkit,” *Nucl.Instrum.Meth.* **A506** (2003) 250–303.
- [39] A. Salvucci, “Measurement of muon momentum resolution of the ATLAS detector,” *EPJ Web Conf.* **28** (2012) 12039, [arXiv:1201.4704 \[physics.ins-det\]](#).
- [40] **ATLAS** Collaboration, G. Aad *et al.*, “Expected Performance of the ATLAS Experiment - Detector, Trigger and Physics,” [arXiv:0901.0512 \[hep-ex\]](#).

- [41] J. Alwall, M. Herquet, F. Maltoni, O. Mattelaer, and T. Stelzer, “MadGraph 5 : Going Beyond,” *JHEP* **06** (2011) 128, [arXiv:1106.0522](https://arxiv.org/abs/1106.0522) [[hep-ph](#)].
<http://arxiv.org/abs/1106.0522>.
- [42] P. Meade and M. Reece, “BRIDGE: Branching ratio inquiry / decay generated events,” [arXiv:hep-ph/0703031](https://arxiv.org/abs/hep-ph/0703031) [[hep-ph](#)].